Pergamon

Int. J. Multiphase Flow Vol. 23, No. 5, pp. 927–944, 1997

Printed in Great Britain
PII: S0301-9322(97)00018-9
0301-9322/97 $17.00 + 0.00

EULERIAN SIMULATION OF BUBBLE FORMATION AT A JET IN A TWO-DIMENSIONAL FLUIDIZED BED

A. BOEMER, H. QI and U. RENZ

Lehrstuhl für Wärmeübertragung und Klimatechnik, RWTH Aachen, Eilfschornsteinstr. 18, D-52056 Aachen, Germany

(Received 14 November 1995; in revised form 19 February 1997)

Abstract—A promising method to describe the fluid dynamics of highly loaded particle flows is the Eulerian representation. In this approach, the solid phase is treated as a continuum, although physically it consists of individual particles. This is possible by using physical models derived from the kinetic theory of granular flow. Central to these models is the so-called granular temperature, representing the specific fluctuating kinetic energy of the particles. In this paper, several forms proposed for these models are summarized and different descriptions of granular temperature are investigated. Furthermore, an alternative approach derived from soil mechanics is tested. Measurements of a two-dimensional bubbling bed found in literature are finally used to verify the results. © 1997 Elsevier Science Ltd.

Key Words: Eulerian simulation, fluid dynamics, gas–solid, kinetic theory, bubbling fluidized bed

1. INTRODUCTION

Gas–solid multiphase systems can be found in many applications of the chemical and power industry. Computer simulations are turning out to be a powerful tool to understand and design such processes. In case of high solid loadings, e.g. in fluidized beds, the simulation procedure should be based on the Eulerian approach, which is the subject of this paper.

The development of the Eulerian approach including kinetic theory for granular flows has started already in the 1980s by Savage and Jeffrey (1981) and others. However, the improvement of computer power in the present decade was needed to allow the simulation of actual gas–solid flows. This induced interest and the basic theory was further developed, e.g. by Ding and Gidaspow (1990), Balzer and Simonin (1993), and Syamlal *et al.* (1993). Although there already exist several publications on this subject, a comparison of the different approaches, including a verification of the resulting flow patterns with measurements, is still missing. The present paper tries to contribute to this task.

In contrast to the Lagrangian approach, which considers each particle separately, in the Eulerian approach all particles in a computational cell are handled as a continuum. Thus, the gas and solid phases can be described by similar mass and momentum balances. These balances are presented in section 2.1; their coupling by a drag function in section 2.2. The physical models needed to treat the solid phase as a continuous fluid are discussed in section 2.3. These models require the granular temperature as a parameter. Hence, different approaches to determining this parameter are investigated in section 2.4. The solution procedure is briefly described in section 3.1, followed in section 3.2 by a presentation of the simulations performed, including a comparison with measured data.

2. BASIC EQUATIONS

2.1. The Eulerian balances

The accumulation of mass in each phase is balanced by the convective mass fluxes (i = gas, solids):

$$\frac{\partial}{\partial t}(\epsilon_i \rho_i) + \nabla \cdot (\epsilon_i \rho_i \mathbf{v}_i) = 0, \qquad [1]$$

where ϵ_i is the volume fraction, ρ_i the density, and $\mathbf{v}_i$ the mean velocity vector.

For the investigations described in this paper, mass exchange between the phases, e.g. due to pyrolysis or combustion, is not considered. According to Newton's second law, for each phase the change of momentum equalizes the net force on a domain. In gas–solid fluidized beds the forces include:

- Viscous force $\nabla\cdot\bar{\bar{\tau}}_i$ ($\bar{\bar{\tau}}_i$ describes the viscous stress tensor)
- Body force $\epsilon_i\rho_i\boldsymbol{g}$
- Solid pressure force ∇p_S^* (solid phase)
- Static pressure force $\epsilon_i\nabla_p$
- Interphase force (drag) ($\beta\cdot(\mathbf{v}_G-\mathbf{v}_S)$ β is the interphase drag force).

Other forces, such as added mass effect, lift force, and Basset force, can assumed to be negligible (Albråten 1982; Anderson 1991). Thus, one obtains the momentum balances of the two phases: solids:

$$\frac{\partial}{\partial t}(\epsilon_S\rho_S\mathbf{v}_S)+\nabla\cdot(\epsilon_S\rho_S\mathbf{v}_S\mathbf{v}_S)=\nabla\cdot\bar{\bar{\tau}}_S+\epsilon_S\rho_S\boldsymbol{g}-\nabla p_S^*-\epsilon_S\nabla p+\beta\cdot(\mathbf{v}_G-\mathbf{v}_S), \quad [2]$$

gas:

$$\frac{\partial}{\partial t}(\epsilon_G\rho_G\mathbf{v}_G)+\nabla\cdot(\epsilon g\rho_G\mathbf{v}_G\mathbf{v}_G)=\nabla\cdot\bar{\bar{\tau}}_G+\epsilon_G\rho_G\boldsymbol{g}-\epsilon_G\nabla\mathrm{p}-\beta\cdot(\mathbf{v}_G-\mathbf{v}_S) \quad [3]$$

with

$$\bar{\bar{\tau}}_i=2\mu_i^*\bar{\bar{D}}_i+\left(\lambda_i^*-\tfrac{2}{3}\mu_i^*\right)\cdot\mathrm{tr}(\bar{\bar{D}}_i)\bar{\bar{I}} \quad [4]$$

and

$$\bar{\bar{D}}_i=\tfrac{1}{2}\left[\nabla\mathbf{v}_i+(\nabla\mathbf{v}_i)^{\mathrm{T}}\right]. \quad [5]$$

With $\epsilon_G=1$ and $\beta=0$ [3] is commonly called the Navier–Stokes equation.

This set of equations with the static pressure p appearing in the momentum equation of both phases is used by most of the researchers working on Eulerian simulation of two phase flows, e.g. Ding and Gidaspow (1990), Balzer and Simonin (1993), Syamlal *et al.* (1993), Löfstrand *et al.* (1995). An alternative approach was proposed by Bouillard *et al.* (1989). They claimed that [2] may be numerically unstable because the problem is ill-posed. This could be avoided if the static pressure term is taken out of the solid phase momentum balance and put completely into the gas phase momentum balance. To satisfy Archimedes' principle they had to increase the drag term. This led to:
solids:

$$\frac{\partial}{\partial t}(\epsilon_S\rho_S\mathbf{v}_S)+\nabla\cdot(\epsilon_S\rho_S\mathbf{v}_S\mathbf{v}_S)=\nabla\cdot\bar{\bar{\tau}}_S+\epsilon_S\rho_S\boldsymbol{g}-\nabla p_S^*+\frac{\beta}{\epsilon_G}\cdot(\mathbf{v}_G-\mathbf{v}_S), \quad [6]$$

gas:

$$\frac{\partial}{\partial t}(\epsilon_G\rho_G\mathbf{v}_G)+\nabla\cdot(\epsilon_G\rho_G\mathbf{v}_G\mathbf{v}_G)=\nabla\cdot\bar{\bar{\tau}}_G+\epsilon_G\rho_G\boldsymbol{g}-\nabla p-\frac{\beta}{\epsilon_G}\cdot(\mathbf{v}_G-\mathbf{v}_S). \quad [7]$$

The set of momentum balances described by [2] and [3], has been called *Hydrodynamic Model A*, and the alternative, [6] and [7], *Hydrodynamic Model B*. The differences resulting from this modification are discussed in section 3.2.2. below.

2.2. *Interphase force*

In order to couple the two momentum balances, a model for the interphase force is required. For the simulations presented in this paper, the drag function of Syamlal *et al.* (1993) is used. It is based on results of Richardson and Zaki (1954), Dalla Valle (1948), and Garside and Al-Dibouni (1977)

$$\beta = \tfrac{3}{4} C_D \cdot \frac{\epsilon_S \epsilon_G \rho_G}{V_r^2 d_S} \cdot |\mathbf{v}_G - \mathbf{v}_S|. \qquad [8]$$

The drag coefficient C_D is evaluated from

$$C_D = \left(0.63 + 4.8 \cdot \sqrt{\frac{V_r}{\mathrm{Re}}}\right)^2 \qquad [9]$$

with

$$V_r = \tfrac{1}{2}\left(a - 0.06\,\mathrm{Re} + \sqrt{(0.06\,\mathrm{Re})^2 + 0.12\,\mathrm{Re}\,(2b - a) + a^2}\right) \qquad [10]$$

$$a = \epsilon_G^{4.14} \qquad [11]$$

$$b = \begin{cases} 0.8\epsilon_G^{1.28} & \text{if } \epsilon_S \geqslant 0.15 \\ \epsilon_G^{2.65} & \text{if } \epsilon_S < 0.15 \end{cases} \qquad [12]$$

and the Reynolds number defined as

$$\mathrm{Re} = \frac{d_S \rho_G \cdot |\mathbf{v}_G - \mathbf{v}_S|}{\mu_G}. \qquad [13]$$

Alternative formulae have been proposed by Ding and Gidaspow (1990), and Di Felice (1994) and give similar results. An equation of Ma and Ahmadi (1990) agrees in the dilute region but differs in the dense regime. These models are compared in Boemer *et al.* (1995) and Löfstrand *et al.* (1995). They are applicable if the distribution of particles in a computational cell can be assumed to be homogeneous, e.g. in bubbling fluidized beds, whereas modifications are needed to account for clusters smaller than a computational cell, e.g. in circulating fluidized beds (O'Brien and Syamlal 1993).

2.3. *Solid phase properties*

In order to adapt the Navier–Stokes equation originally derived for a continuous fluid, physical models are required to describe:

- the solid pressure $p_S^* = p_S \cdot \epsilon_S$
- the solid bulk viscosity $\lambda_S^* = \lambda_S \cdot \epsilon_S$
- the solid shear viscosity $\mu_S^* = \mu_S \cdot \epsilon_S$.

Several empirical approaches have been developed which can be used under certain conditions (see, e.g. Massoudi *et al.* 1992; Dasgupta *et al.* 1994). Furthermore, there exists an alternative approach called the kinetic theory of granular flows. Since this theory makes a general description of the occurring phenomena possible, it should be preferred to the empirical approaches. It is based on the kinetic theory of gases (Chapman and Cowling 1970) and was developed mainly by Savage and Jeffrey (1981), Jenkins and Savage (1983), and Lun *et al.* (1984). The macroscopic behaviour of the solid phase is thus described by statistical expressions of collisions and fluctuating motions of the particles. By means of this theory the normal forces due to particle interactions can be

expressed as solid pressure and bulk viscosity, and the tangential forces are summarized in a term called shear viscosity. The most important restrictions of this theory are:

- spherical, smooth, and nearly elastic particles
- identical particles (diameter, density, restitution coefficient)
- enough particles to allow the utilisation of the laws of statistical mechanics
- binary collisions.

The resulting models are listed below, a more detailed discussion is given in Boemer *et al.* (1995).

2.3.1. Solid pressure. The solid pressure represents the normal force due to particle interactions and can be calculated from Lun *et al.* (1984)

$$p_S^* = p_S\epsilon_S = \epsilon_S\rho_S\Theta_S\cdot(1+2g_0\epsilon_S\cdot(1+e)). \qquad [14]$$

The radial distribution function g_0 and granular temperature Θ_S are discussed below.

2.3.2. Solid bulk viscosity. The bulk viscosity is a measure of the resistance of a fluid to compression. Lun *et al.* (1984) proposed a formula which is commonly used

$$\lambda_S^* = \lambda_S\epsilon_S = \tfrac{4}{3}\epsilon_S^2\rho_S d_S g_0\cdot(1+e)\cdot\sqrt{\frac{\Theta_S}{\pi}}. \qquad [15]$$

2.3.3. Solid shear viscosity. There is general agreement in the literature on how to express the solid pressure and bulk viscosity but different expressions for the shear viscosity are used. It is difficult to discriminate between these different models since few detailed measurements exist. However, the models differ mainly in the dilute region (say, $\epsilon_S < 0.3$) which is of minor importance in bubbling fluidized beds. The model of Gidaspow *et al.* (1992) comes closest to the measurements of Gidaspow *et al.* (1989) and is tested here

$$\mu_S^* = \mu_S\epsilon_S = \tfrac{4}{5}\epsilon_S^2\rho_S d_S g_0\cdot(1+e)\cdot\sqrt{\frac{\Theta_S}{\pi}}+\frac{2\cdot\frac{5\sqrt{\pi}}{96}\rho_S d_p\sqrt{\Theta_S}}{(1+e)\cdot g_0}\cdot\left[1+\tfrac{4}{5}g_0\epsilon_S\cdot(1+e)\right]^2. \qquad [16]$$

For $\epsilon_S \to 0$ it is equal to the expression given by Chapman and Cowling (1970). As discussed in Boemer *et al.* (1995), alternatives were proposed by Syamlal *et al.* (1993) and Balzer and Simonin (1993). The latter is also included in one of the test cases presented below, it reads

$$\mu_S^* = \tfrac{4}{5}\epsilon_S^2\rho_s d_S g_0\cdot(1+e)\cdot\sqrt{\frac{\Theta_S}{\pi}}+\frac{\Theta_S\cdot(\rho_S\epsilon_S)^2}{2\beta+\rho_S\epsilon_S^2\cdot\frac{(1+e)\cdot(3-e)}{5}\cdot\frac{6}{d_S}\cdot\sqrt{\frac{16\Theta_S}{\pi}}}. \qquad [17]$$

Both equations give similar results in the dense region but may differ in the dilute region.

2.3.4. Extreme regimes: dense and dilute. If the solid phase is in the packed bed state ($\epsilon_S \approx 0.6$), the stresses are dominated by interparticle friction rather than by collisions and fluctuating motion. Jackson (1983) investigated soil mechanics phenomena and proposed to use the stress tensor of Sokolovski (1965) for a granular material which is about to yield. This tensor is (here, for simplicity, the two-dimensional version)

$$\overline{\overline{\tau_{S,f}}} = \begin{pmatrix} \sigma\cdot(1+\sin\phi\cos 2\gamma) & -\sigma\cdot(\sin\phi\sin 2\gamma) \\ -\sigma\cdot(\sin\phi\sin 2\gamma) & \sigma\cdot(1-\sin\phi\cos 2\gamma) \end{pmatrix} \qquad [18]$$

and fulfils the Coulomb yield criterion (Jackson 1983). It contains the angle of internal friction ϕ (Johnson and Jackson (1987) proposed $\phi = 25°$) and the angle γ between the direction of the major principal stress and the x-axis. The latter can be derived from geometrical considerations. σ is the normal stress component which is the solid pressure in our case. Syamlal *et al.* (1993) showed that this stress tensor [18] is equal to that used in the momentum balance of the solid phase [2]

$$\nabla\cdot\overline{\overline{\tau_S}} - \nabla p_S^* \equiv \nabla\cdot\overline{\overline{\tau_{S,f}}} \qquad [19]$$

if the following expression for the solid shear viscosity is used (two dimensional version)

$$\mu_S^* = \frac{p_S^* \cdot \sin\phi}{2\sqrt{\frac{1}{6}\left(\left(\frac{\partial u_S}{\partial x}-\frac{\partial v_S}{\partial y}\right)^2+\left(\frac{\partial v_S}{\partial y}\right)^2+\left(\frac{\partial u_S}{\partial x}\right)^2\right)+\frac{1}{4}\left(\frac{\partial u_S}{\partial y}+\frac{\partial v_S}{\partial x}\right)^2}} \equiv \mu_{S,f}^*. \quad [20]$$

This derivation is valid if the solid volume fraction is constant and if the principal stresses of both tensors in [19] have the same direction. The first assumption is reasonable in the packed bed state of particles ($\epsilon_S = \epsilon_{S,max}$); the latter was shown to be the case by Jackson (1983).

In the very dilute region, the Lagrangian approach might be preferred to the Eulerian approach since it handles each particle separately. However, it is difficult to find a limit of applicability for the approaches. The maximum number of particles for the Lagrangian approach is limited by the computer power. For example, a solid volume fraction of $\epsilon_S = 0.01$ means that about 15×10^7 particles or groups of particles per m^3 have to be tracked ($d_S = 0.5$ mm). Concerning the Eulerian approach, Kuipers (1990) argued that at least 10^4 particles per volume are required for a statistical variation of less than 1%. This leads to

$$\epsilon_{S,min} = \frac{10^4 \pi d_S^3}{6V}. \quad [21]$$

For the simulations discussed below ($d_S = 0.5$ mm, typical cell size $0.01 \times 0.01 \times 1$ m^3), $\epsilon_{S,min}$ becomes 6.5×10^{-3}. Another possibility is to consider that fluctuating motions of particles are limited by the surrounding walls. Thus, the diameter of the apparatus can be regarded as the maximum mean free path. Gidaspow (1994) proposed a formula to calculate the mean free path. With this, one obtains

$$\epsilon_{s,min} = \frac{1}{6\sqrt{2}} \cdot \frac{d_S}{d_{app}}. \quad [22]$$

This equation gives $\epsilon_{S,min} = 10^{-4}$ for the geometry of the test case ($d_{app} = 0.57$ m). Since [22] is independent of the chosen cell size, it was decided to implement it into the code. If the local solid volume fraction obtained from the mass balances is below this limit, the result from [22] is used to calculate the solid phase properties. By means of this simplification unrealistic results in the extreme dilute region can be avoided.

2.3.5. Radial distribution function. The solid phase models discussed above are based on two crucial properties, namely the radial distribution function g_0 and granular temperature Θ_S. The radial distribution function is a measure for the probability of interparticle contact. The model used in this paper was proposed by Ding and Gidaspow (1990).

$$g_0 = -\frac{3}{5} \cdot \left[1-\left(\frac{\epsilon_S}{\epsilon_{s,max}}\right)^{\frac{1}{3}}\right]^{-1}. \quad [23]$$

It was developed with respect to collision rates investigated by Alder and Wainwright (1960). Alternative approaches (Carnahan and Starling 1969; Lun and Savage 1986; Balzer and Simonin 1993) are discussed in Boemer *et al.* (1995).

Modelling of the granular temperature is discussed in section 2.4.

2.3.6. Verification of the solid pressure model. The experiments of Campbell and Wang (1991) can be used to verify the solid pressure model and to estimate the range of granular temperature occurring in a bubbling fluidized bed. They used a differential pressure transducer to measure the solid pressure near the wall of a $0.127 \times 0.127 \times 1.22$ m^3 bubbling fluidized bed. Varying the solids density and diameter they found exactly what [14] predicts: no influence of the diameter and a linear dependency on the solid density. The data depicted in figures 1 and 2 were obtained with glass beads ($\rho_S = 2440$ kg/m^3, $d_S = 0.5$ mm) similar to those used at the test cases described below. The solid pressure calculated according to [14] (including [23] with $\epsilon_{S,max} = 0.6$) is plotted in figure 1. Campbell and Wang (1991) varied the solid volume fraction by changing the fluidizing velocity. Thus, the granular temperature was not constant in their measurements. At lower solid volume

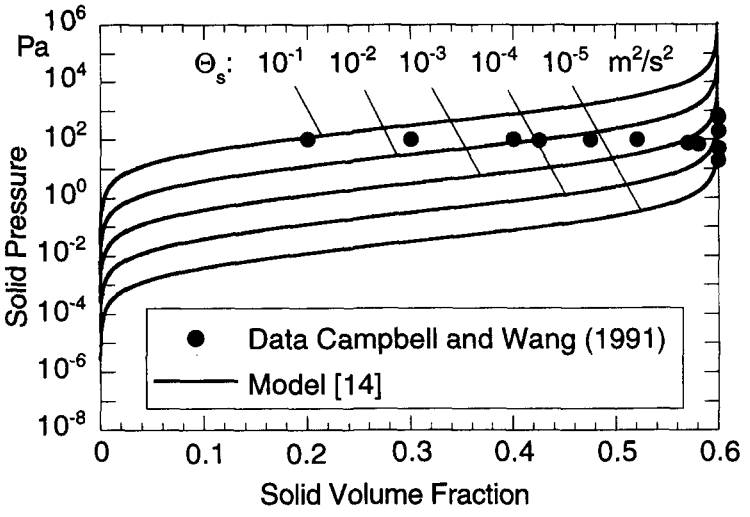

Figure 1. Verification of the solid pressure model.

fractions, the solid fluctuations and correspondingly the granular temperature can be assumed to be higher due to the higher gas velocity. The solid pressure increases both with the intensity (granular temperature), and with the number (solid volume fraction) of solids interactions. Comparing the results of the model with the measured data implies $10^{-5} < \Theta_S < 0.1\ m^2/s^2$ to be a suitable range of granular temperature. As figure 1 shows, the granular temperature has a strong influence on the solid pressure level. Variations by four orders of magnitude are possible.

To further verify the solid pressure model in the framework of the code, a complete simulation of one of the bubbling bed experiments of Campbell and Wang (1991) was performed ($u_0 = 0.4$ m/s). A period of 10 s was simulated and an average of the last 9 s was used to compare with the experimental data. The models implemented in this simulation are those listed for test case 4 in table 1. The results are depicted in figure 2 and demonstrate reasonable agreement between the measured and calculated solid pressure near the wall. In the simulation, bubbles were observed to touch the sidewalls. Inside these bubbles, the solid pressure is much smaller than in the surrounding emulsion. Due to the short averaging time, these bubbles caused the scatter in the simulation results. However, both simulation and experiment show an increase of solid pressure with height caused by the solids fluctuating motion induced by the growing bubbles.

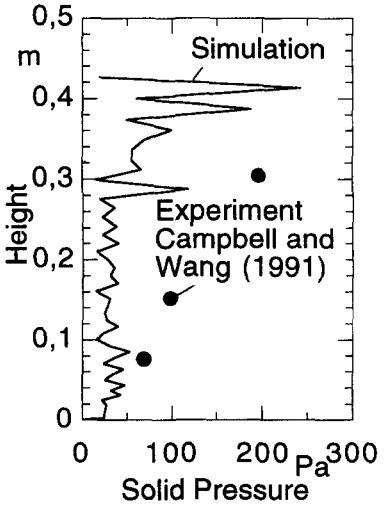

Figure 2. Solid pressure near the wall.

Table 1. Models used for the simulations

Test case	Granular temperature Θ_S	Shear viscosity μ_S^*	Hydrodynamic model (see 2.1)
1	Constant 10^{-4} m^2/s^2	Gidaspow *et al.* (1989), [16]	A
2	Constant 9×10^{-3} m^2/s^2 (mean value from test case 6)	Gidaspow *et al.* (1989), [16]	A
3	Algebraic formula [36]	Gidaspow *et al.* (1989), [16]	A
4	[25] with k_Θ from Gidaspow *et al.* (1992), [30] and [31]	Gidaspow *et al.* (1989), [16]	A
5	[25] with k_Θ from Balzer and Simonin (1993), [31] and [32]	Balzer and Simonin (1993), [17]	A
6	[25] with k_Θ from Syamlal *et al.* (1993), [28]	Gidaspow *et al.* (1989), [16]	A
7	[25] with k_Θ from Gidaspow *et al.* (1992), [30] and [31]	If $\epsilon_S < 0.59$: Gidaspow *et al.* (1989), [16] If $\epsilon_S \geqslant 0.59$: soil mechanics [20] with limit: $\mu_S^* < 1000$ Pa·s	A
8		Same as test case 7, but limit $\mu_S^* < 100$ Pa·s	
9	[25] with k_Θ from Gidaspow *et al.* (1992)	Gidaspow *et al.* (1989), [16]	B

2.4. *Solids fluctuating motion: granular temperature*

The kinetic energy of particles is proportional to the square of their velocity. This velocity can be divided into a mean $\mathbf{v}_S$ and a fluctuating part $\mathbf{v}_S'$. The mean velocity is accounted for in the momentum balance. Similar to the treatment of turbulent gas flows, a model is necessary to account for the local instantaneous fluctuating velocity. This can be achieved by means of the kinetic theory of granular flow. Equivalent to the thermodynamic temperature for gases, the granular temperature can be introduced to represent the energy associated with the fluctuating velocity of particles. Assuming isotropy of the fluctuating motions the kinetic energy of the solid fluctuation can be formulated

$$E_S = \tfrac{1}{2} m_S \mathbf{v}_S'^2 \equiv \tfrac{3}{2} m_S \Theta_S \qquad [24]$$

with the particle mass m_S and the granular temperature defined by $\Theta_S = \frac{1}{3}\mathbf{v}_S'^2$. Models to calculate the granular temperature are discussed in the following subsections.

2.4.1. Granular temperature from partial differential equation. A balance of the solids fluctuating energy can be written as follows (see, e.g. Ding and Gidaspow 1990; Syamlal *et al.* 1993; Balzer and Simonin 1993)

$$\tfrac{3}{2}\left[\frac{\partial}{\partial t}(\epsilon_S \rho_S \Theta_S) + \nabla\cdot(\epsilon_S \rho_S \Theta_S)\mathbf{v}_S\right] = \left(-p_S^*\bar{\bar{I}} + \bar{\bar{\tau}}_S\right) : \nabla \mathbf{v}_S + \nabla\cdot(k_\Theta \nabla \Theta_S) - \gamma_\Theta + \Phi_\Theta. \qquad [25]$$

The left-hand side of [25] is the net change of fluctuating energy. It is equal to the sum of the right hand side terms described below.

The *generation* of fluctuating energy by local acceleration of the particles is accounted for by the term $(-p_S^*\bar{\bar{I}} + \bar{\bar{\tau}}_S) : \nabla \mathbf{v}_S$ which includes solid pressure and the shear tensor $\bar{\bar{\tau}}_S$ as defined by [4].

Diffusion of fluctuating energy can be described in the usual way by a gradient of the granular temperature with a diffusion coefficient k_Θ. The diffusion coefficient can be formulated for the dilute and the dense region.

$$k_\Theta = k_{\Theta,\text{dilute}} + k_{\Theta,\text{dense}}. \qquad [26]$$

In principle, the term $k_{\Theta,\text{dilute}}$ mainly accounts for the kinetic part of the diffusion coefficient, whereas $k_{\Theta,\text{dense}}$ is dominated by the collisional influence. Similar to the shear viscosity description, the

equations for the diffusion coefficient proposed in literature differ, although all of them are derived from kinetic theory.

Lun *et al.* (1984)

$$k_{\Theta,\text{dilute}} = \tfrac{25}{16}\frac{d_S\rho_S\sqrt{\pi\Theta_S}}{g_0\eta(41-33\eta)}\left[1+\tfrac{12}{5}\eta^2(4\eta-3)\epsilon_S g_0\right] \quad [27]$$

$$k_{\Theta,\text{dense}} = \tfrac{15}{4}\frac{d_S\rho_S\epsilon_S\sqrt{\pi\Theta_S}}{(41-33\eta)}\left[1+\tfrac{12}{5}\eta^2(4\eta-3)\epsilon_S g_0+\tfrac{16}{15\pi}(41-33\eta)\eta\epsilon_S g_0\right] \quad [28]$$

with the abbreviation

$$\eta = \tfrac{1}{2}(1+e). \quad [29]$$

Syamlal *et al.* (1993) employed this approach but neglected $k_{\Theta,\text{dilute}}$.

Gidaspow *et al.* (1992) used an expression based on the work of Chapman and Cowling (1970)

$$k_{\Theta,\text{dilute}} = \tfrac{75}{192}\frac{\rho_S d_S\sqrt{\pi\Theta_S}}{(1+e)g_0}\left[1+\tfrac{6}{5}(1+e)g_0\epsilon_S\right]^2 \quad [30]$$

$$k_{\Theta,\text{dense}} = 2\epsilon_S^2\rho_S d_S g_0(1+e)\sqrt{\frac{\Theta_S}{\pi}}. \quad [31]$$

Balzer and Simonin (1993) also utilise [31] for the dense region, and for the dilute region they proposed

$$k_{\Theta,\text{dilute}} = \tfrac{5}{9}\frac{\epsilon_S^2\rho_S^2\Theta_S}{\beta}\left[1+\tfrac{5}{9}\frac{\epsilon_S^2\rho_S\cdot(1+e)\,(49-33e)}{\beta d_S}\sqrt{\frac{\Theta_S}{\pi}}\right]^{-1}. \quad [32]$$

Note that the coefficient $k_{\Theta,\text{dilute}}$ of Gidaspow *et al.* (1992) [30] includes collisional influences and, hence, goes to infinity for $\epsilon_S \to \epsilon_{S,\max}$, whereas those of Lun *et al.* (1984) [27] and Balzer and Simonin (1993) [32] are finite small values in case of $\epsilon_S = \epsilon_{S,\max}$.

To get an impression of these approaches, the diffusion coefficients k_Θ are plotted in figure 3 versus solid volume fractions for two granular temperatures. The particles are those of the test case described below ($d_S = 0.5$ mm, $\rho_S = 2660$ kg/m^3, $e = 0.61$), and g_0 from [23] with $\epsilon_{S,\max} = 0.6$ is used. For the drag function β required in [32], [8] with a constant relative velocity of $|\mathbf{v}_G - \mathbf{v}_S| = 1$ m/s

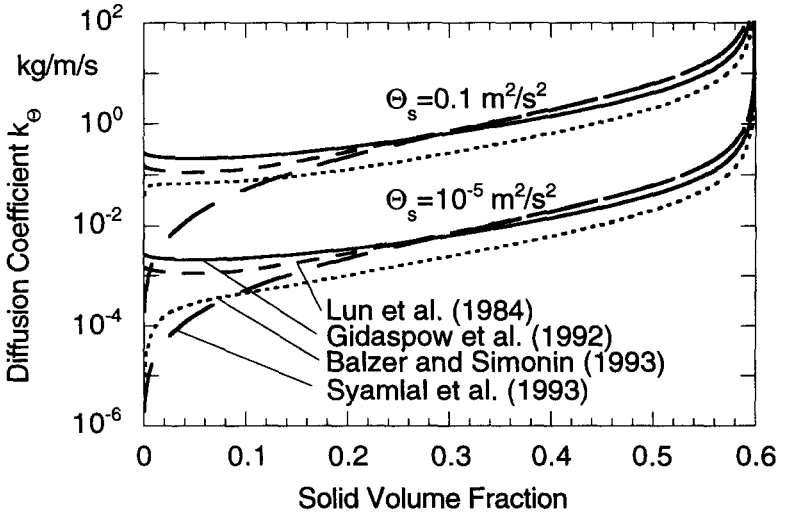

Figure 3. Diffusion coefficient of solids fluctuating energy.

was chosen. However, varying this relative velocity in the typical range has no significant influence on the results. Only in the very dilute region the diffusion coefficient becomes somewhat higher for higher relative velocities. As shown in figure 3, all diffusion coefficients increase with solid volume fraction and granular temperature. In the whole range of solid volume fraction, the approaches of Lun *et al.* (1984) and Gidaspow *et al.* (1992) give similar results. The difference between them gets even smaller if higher restitution coefficients e are used. Neglecting $k_{\Theta,\text{dilute}}$ (Syamlal *et al.* 1993) has the consequence of very low values in the dilute regime ($k_\Theta \to 0$ for $\epsilon_S \to 0$), whereas the equations of Lun *et al.* (1984) and Gidaspow *et al.* (1992) lead to finite values of k_Θ for $\epsilon_S \to 0$. However, in the very dilute regime, the solid phase is no more dominated by kinetic and collisional influences but by the interaction with the gas phase. This is taken into account by Balzer and Simonin (1993) who included the drag function β. Furthermore, the gas phase turbulence may play a major role in the dilute regime if the particles are small enough. In case of low solid volume fractions it may increase k_Θ considerably. However, as discussed above, in case of extremely low solid concentrations the Eulerian approach is questionable in general. Higher solid volume fractions damp gas phase turbulence (Mih 1993; Yang *et al.* 1993) and in bubbling fluidized beds its effect can surely be neglected.

It is difficult to decide which approach is the most appropriate without having special measurements. There are theoretical arguments for all of them. Results of the approaches of Gidaspow *et al.* (1992), [30] and [31], and of Balzer and Simonin (1993), [31] and [32], are discussed in section 3.2.

The *dissipation* of fluctuating energy can be described (Jenkins and Savage 1983)

$$\gamma_\Theta = 3\,(1 - e^2)\epsilon_S^2 \rho_S g_0 \Theta_S \left(\frac{4}{d_S} \sqrt{\frac{\Theta_S}{\pi}} - \nabla \cdot \mathbf{v}_S \right). \qquad [33]$$

Lun *et al.* (1984), and later Syamlal *et al.* (1993) and Balzer and Simonin (1993) neglected the term $\nabla \cdot \mathbf{v}_S$. It may lead to negative dissipation and is neglected in the present investigations, too. A restitution coefficient $e = 1$ has the meaning of an elastic collision without loss of kinetic energy, hence the dissipation becomes zero. With the radial distribution function [23] the dissipation goes to infinity in case of dense packing ($\epsilon_S \to \epsilon_{S,\max}$).

The *exchange* of fluctuating energy between gas and solid phase is usually calculated according to Ding and Gidaspow (1990)

$$\Phi_\Theta = -3\beta\Theta_S. \qquad [34]$$

It accounts for the loss of granular energy due to friction with the gas.

This partial differential equation for granular temperature [25] has the same form as, e.g. the mass and momentum balances and can be numerically solved in the same way (see, e.g. Patankar 1980). However, since this procedure requires considerable additional CPU power, a simpler alternative is investigated and described in the next subsection.

2.4.2. Algebraic formula for granular temperature. Instead of solving the complete differential equation [25], an algebraic expression proposed by Syamlal *et al.* (1993) can be used. They assumed local equilibrium between generation and dissipation of fluctuating energy. Thus, [25] becomes

$$0 = (-\overline{\overline{p_S^*}} + \overline{\overline{\tau_S}}) : \nabla \mathbf{v}_S - \gamma_\Theta. \qquad [35]$$

With [4], [14]–[16] and [33], [35] can be written

$$\Theta_S = \left(\frac{-(K_1\epsilon_S + \rho_S)\cdot \mathrm{tr}\,(\overline{\overline{D_S}}) + \sqrt{(K_1\epsilon_S + \rho_S)^2 \cdot \mathrm{tr}^2(\overline{\overline{D_S}}) + 4K_4\epsilon_S\,[2K_3 \cdot \mathrm{tr}\,(\overline{\overline{D_S^2}}) + K_2 \cdot \mathrm{tr}^2(\overline{\overline{D_S}})\,]}}{2\epsilon_S K_4} \right)^2 \qquad [36]$$

with the abbreviations

$$K_1 = 2(1 + e)\rho_S g_0 \quad [37]$$

$$K_2 = \frac{4}{3\sqrt{\pi}} d_S \rho_S (1 + e)\epsilon_S g_0 - \tfrac{2}{3} K_3 \quad [38]$$

$$K_3 = \frac{d_S \rho_S}{2}\left\{\frac{\sqrt{\pi}}{3(3 - e)}\left[1 + \tfrac{2}{5}(1 + e)(3e - 1)\epsilon_S g_0\right] + \frac{8\epsilon_S}{5\sqrt{\pi}} g_0(1 + e)\right\} \quad [39]$$

$$K_4 = \frac{12(1 - e^2)\rho_S g_0}{d_S\sqrt{\pi}}. \quad [40]$$

Equation [36] is slightly different from the original one used by Syamlal *et al.* (1993) because it includes the kinetic part of the solid pressure. The kinetic part of the shear viscosity in [16] has to be neglected in order to get an algebraic equation. Granular temperature from [36] depends strongly on the local solid velocity gradients included in the strain rate tensor. Since it may go to infinity for $\epsilon_S \to 0$, an upper limit has to be fixed. For $\epsilon_S \to \epsilon_{S,max}$ the granular temperature may become very small, so a minimum value is reasonable to avoid zero solid pressures and viscosities. A suitable range for the granular temperature is discussed in the next subsection.

2.4.3. Typical range of granular temperature. For bubbling fluidized beds, there exist no measured data of solids fluctuating energy. Obviously it is not possible to measure reliable data in a dense suspension. In circulating fluidized beds, the solids loading is much smaller and some data are available. Yang *et al.* (1993) measured RMS solids velocity fluctuations up to $v_S' = 1.4$ m/s ($\Theta_S = 0.65$ m^2/s^2) with a superficial gas velocity of $u_0 = 4.3$ m/s. Pita and Sundaresan (1991) found values up to nearly 400 m^2/s^2 with gas velocities up to 20 m/s. Due to the higher gas velocities, the considerable influence of the gas turbulence, and the smaller and lighter particles in circulating fluidized beds, these values are higher than those to be expected in bubbling fluidized beds.

Moseley and O'Brien (1993) assumed the excess fluidization energy to cause the solids fluctuating motion. They proposed a formula for the average granular temperature of a bubbling fluidized bed

$$\overline{\Theta}_S = \tfrac{1}{3}\frac{k_1 \rho_G}{\epsilon_S \rho_S}(u_0 - u_{mf})^2. \quad [41]$$

The factor k_1 is the fraction of excess fluidization energy going into solids fluctuation energy. The choice of k_1 is arbitrary without detailed measurements but crucial for the results. Since k_1 is defined between 0 and 1, this formula results in $0 < \overline{\Theta}_S < 1.7 \times 10^{-5}$ m^2/s^2 for the test case described below (gas density $\rho_G = 1.276$ kg/m^3, solid density $\rho_S = 2660$ kg/m^3, superficial gas velocity $u_0 = 0.507$ m/s, minimum fluidization velocity $u_{mf} = 0.26$ m/s, minimum fluidation solid volume fraction $\epsilon_S = \epsilon_{S,mf} = 0.598$). Moseley and O'Brien (1993) used $k_1 = 0.0326$ which gives $\overline{\Theta}_S = 5.4 \times 10^{-7}$ m^2/s^2 in this case. However, during operation the mean solid volume fractions will be lower and cause higher values of $\overline{\Theta}_S$. In case of $\epsilon_S \to 0$ the granular temperature [41] goes to infinity.

Combining these findings with the conclusions drawn in section 2.3.6 from experiments of Campbell and Wang (1991), the typical range of granular temperature occurring at bubble formation processes as regarded here is $10^{-5} < \Theta_S < 0.1$ m^2/s^2. This range agrees with the values estimated by Balzer and Simonin (1993). Hence, these limits are applied to the simulations discussed below.

3. SIMULATION

3.1. Solution procedure

In a cooperation between the Lehrstuhl für Wärmeübertragung und Klimatechnik in Aachen, Germany, and FLUENT Europe Ltd in Sheffield, U.K., a computer code is being developed to solve the equations discussed above. Following the suggestion of Syamlal and O'Brien (1989), the solid phase is treated as a compressible fluid in case of $\epsilon_S < \epsilon_{S,max}$ and incompressible if $\epsilon_S = \epsilon_{S,max} = 0.6$. The dependence $\epsilon_S = f(p_S)$ is treated like the dependency $\rho_G = f(p)$ in compressible

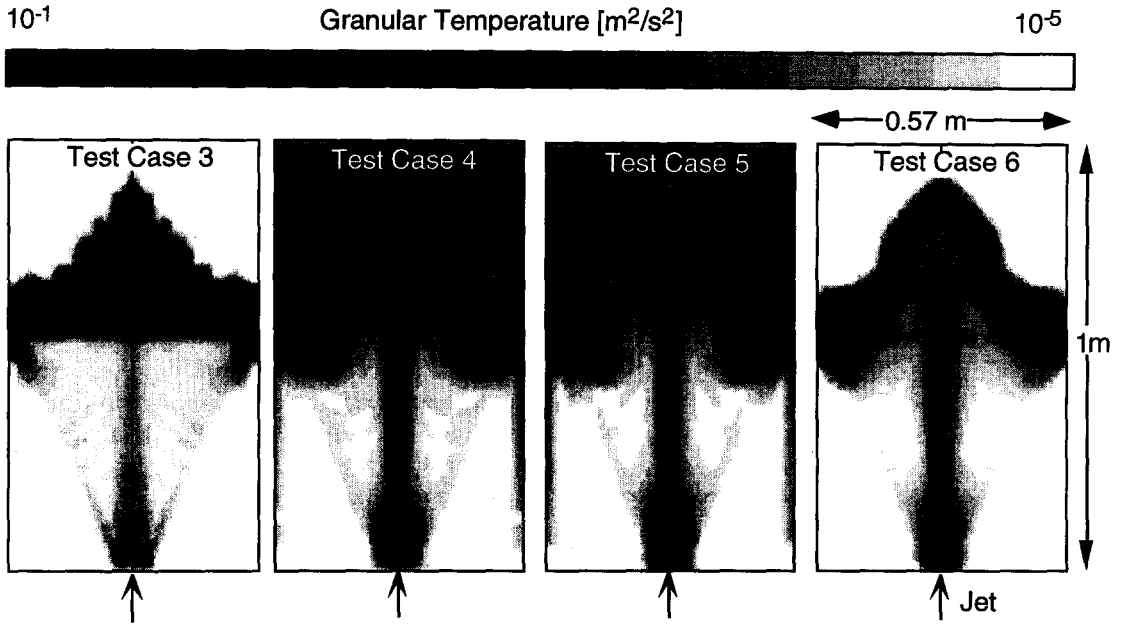

Figure 4. Time averaged (0–2 s) granular temperature.

gas flows (see Patankar 1980). The differential equations are solved implicitly with a TDMA solver. An extension of the SIMPLE scheme of Patankar (1980), called SIMPLE-PEA has been chosen. PEA stands for Partial Elimination Algorithm and was introduced by Spalding (1980). Static pressure correction is executed with a mass balance of the gas phase and a similar solid pressure correction with that of the solid phase. The result of this solid pressure correction is taken to correct the solid velocity, the solid volume fraction, and the fluxes through the cell faces. The solid pressure is calculated by [14], except if $\epsilon_{S,max}$ is going to be reached. in this case the result of the solid pressure correction is used for the solid pressure, too. Thus, further flow of particles into a filled cell is terminated and a solid volume fraction higher than $\epsilon_{S,max}$ is avoided. Solid volume fractions are obtained by means of a combined mass balance of both phases. To avoid numerical problems, the result is limited to a value of $\epsilon_{S,min} = 10^{-6}$. At the present stage of development, turbulence modelling of the gas phase neglects the influence of particles.

3.2. Test cases

Experimental investigations of the bubble formation at a jet within a fluidized bed by Kuipers (1990) can be used to verify the results of the simulation. These were carried out on a two-dimensional test rig of 0.015 × 0.57x1 m^3 size. In the centre, a jet with an outlet velocity of 10 m/s was introduced through a rectangular mouth of 0.015 × 0.015 m^2. The rest of the bed area was fluidized with its minimal fluidization velocity of 0.25 m/s. The device was filled up to a height of 0.5 m with glass beads (500 μm, 2660 kg/m^3). A symmetry plane assuming no crossing mass fluxes has been applied at the centreline to minimise calculation time. This domain has been divided into 31 × 80 computational cells. No significant difference was found at a test-calculation with a doubled grid. Near the wall and in the jet region the grid spacing has been refined. At the walls, no-slip boundary condition has been applied for both phases (Dirichlet boundary condition), whereas at inlet and outlet zero-gradient boundary conditions (Neumann boundary condition) have been used. Both the jet and fluidization inflow are free of particles. Turbulence of the gas phase is neglected. The average calculation time was about 8 h on a HP 737 workstation for 0.1 s of simulation.

According to Geldart (1973), the particles used here belong to group B, close to group D. This means, formation of large spherical bubbles can be expected to start immediately after the minimum fluidization velocity is exceeded. The formula of Grace and Lim (1987) predicts a

permanent jet if the orifice diameter is smaller than 25.4 times the particle diameter. In the setup regarded here, this ratio is equal to 30 which means bubbles will occur.

An overview of the performed simulations is given in table 1.

Calculated granular temperatures from different models are compared in figure 4. In the dense region in the bottom corners, high collision rates cause strong dissipation of fluctuating energy, and all models reach the minimum granular temperature limit. The maximum is reached at the splash zone and near the gas jet, where strong acceleration generates fluctuating energy. Near the walls, where the velocity gradients are high, all simulations predict a small region with a solid volume fraction slightly lower than $\epsilon_{s,max}$ and a granular temperature above the lower limit. Due to interpolation and the limited number of filled contours, this region is visible only for test cases 4 and 5.

If the transport of fluctuating energy is neglected, as done in test case 3 by applying the algebraic formula [36], distinct local extrema of the granular temperature are found. These spots are smeared by the various transport phenomena accounted for in test cases 4, 5 and 6 by the partial differential equation [25]. In the plot of test case 3, the horizontal border between high and low granular temperatures at the initial bed surface is due to high granular temperatures during the first 0.5 seconds of the simulation caused by high velocity gradients at the bed surface. This effect can be observed at all the test cases, but the high granular temperatures do not occur in test cases 4, 5 and 6 since, again, the high amount of fluctuating energy produced by the velocity gradients is transported by diffusion and thus smeared.

Test cases 4 and 5 give nearly identical results. Obviously the approaches of Gidaspow *et al.* (1992) and Balzer and Simonin (1993) are similar under these conditions. The only difference between test case 4 and 6 is the neglection of the first diffusion coefficient $k_{\Theta,dilute}$ ([27], compare figure 3) in test case 6. This term accounts for diffusion of fluctuating energy from the splash zone into the very dilute freeboard region. Since the granular temperature is the fluctuating energy per

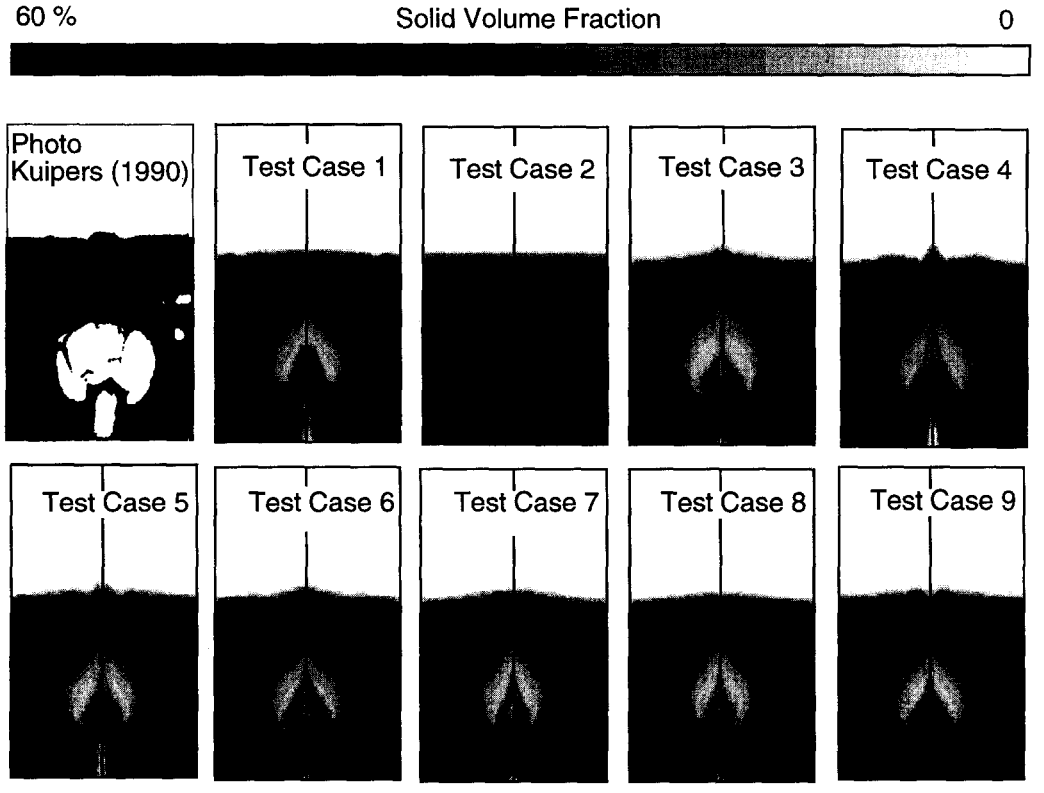

Figure 5. Solid volume distribution 0.4 s after starting the jet for different test cases (parameters see table 1).

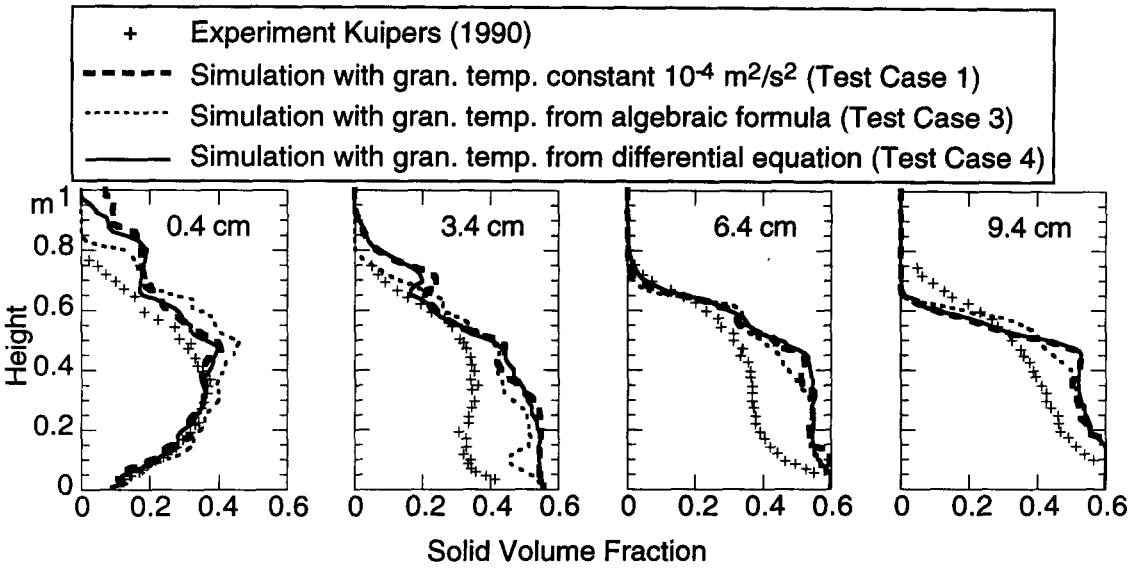

Figure 6. Time-averaged solid volume fractions at different distances from the centerline, variation of granular temperature models.

mass of particles, it becomes very high there. As will be discussed below, these high values have no significant effect on the overall results.

3.2.1. Qualitative verification. The solids distribution 0.4 s after starting the jet is depicted in figure 5. The photo of Kuipers (1990) can be compared with the calculated solid volume fractions. The first simulation (test case 1) was performed with an estimated constant value of $\Theta_S = 10^{-4}$ m^2/s^2. The result looks reasonable, but such a simulation depends strongly on the chosen value. Other calculations with a value of $\Theta_S = 9 \times 10^{-3}$ m^2/s^2 (test case 2), which is the average of the granular temperatures obtained in test case 6, or with $\Theta_S = 10^{-5}$ m^2/s^2 (not shown in figure 5) gave completely unrealistic solid distributions. Except these, all other simulations show a bubble shape similar to that measured by Kuipers (1990). All simulations predict a slightly lower bed height compared to the photograph. This could be due to small bubbles (visible on the right-hand side of the photo) caused by unavoidable small asymmetries in the experimental setup. Furthermore, a lower value than the assumed maximum solid volume fraction, $\epsilon_{S,max} = 0.6$, would automatically increase the calculated bed height. In the photo, the second bubble is already visible at $t = 0.4$ s. Test cases 1, 4 and 5 agree with this observation, at the other test cases it is formed a little later. Test cases 7 and 8 predicted a somewhat leaner bubble compared to the others. This is due to the higher shear viscosity coming from the frictional approach [19]. No difference is found between the images of test case 7 and 8 which shows that the choice of the maximum limit of the shear viscosity coming from the soil mechanics model is not crucial. Concerning the shape of the first bubble, the two Hydrodynamic Models A (test case 4) and B (test case 9), presented in section 2.1, give similar results. Furthermore, neglecting the term for the dilute region in the fluctuating energy diffusion coefficient, as proposed by Syamlal *et al.* (1993) shows no significant effect (cf. test cases 4 and 6). However, test cases 4 and 5 with the approaches of Gidaspow (1992) and Balzer and Simonin (1993), respectively, predict the bubble shapes that agree best with the experimental observation.

3.2.2. Quantitative verification. Kuipers (1990) additionally measured the time-averaged local solid volume fraction by means of an optical probe. The time of averaging was 60 s, whereas only 2 s were simulated due to the high computation cost.

A variation of the three granular temperature models (constant, algebraic expression, partial differential equation) is depicted together with these measurements in figure 6. Test cases 5 and 6 are not depicted in this figure. Their results are similar to those of test case 4, which once more indicates that $k_{\Theta,dilute}$ can be neglected in this bubbling bed case (Syamlal *et al.* 1993). For all the cases considered, experiment and simulations give similar results. A clear influence of the granular

temperature model is found only in the centre of the apparatus. This is due to the high solid volume fraction in the bed which causes dissipation of fluctuating energy down to the minimum value, regardless of the chosen model. Test case 1 shows that a constant granular temperature of $\Theta_S = 10^{-4}\ m^2/s^2$ is a good choice in this case. As already concluded from figure 5, the chosen maximum solid volume fraction of 0.6 seems to be too high. At most of the locations, the predicted solids concentration in the bed is higher than the measured one.

Compared to the data measured 0.4 cm from the centreline, in all three simulations the particles are splashed too high into the freeboard. Especially test case 1 leads to unrealistic results. This problem has also been observed by Gamwo *et al.* (1995), who called it the "fountain problem" and proposed to use Hydrodynamic Model B instead of the usual Model A (see chapter 2.1) to overcome it. This model is tested in test case 9. Another possibility to overcome the fountain problem is to consider interparticle friction in the dense region by using the shear viscosity [20] from solid mechanics. This model is engaged in test cases 7 and 8 for solid volume fractions higher than 0.59. In this state, the solid pressure may be very high, which leads to high viscosities. Test case 8 is not depicted in figure 7 since its results are identical to those of test case 7. In fact these two models predict a drastic decrease of the solid volume fraction at a certain height, as visible in figure 7. Due to the strong shear forces obtained from the frictional approach (test case 7), the particles are hindered in leaving the bed. In the bed region, 3.4 cm from the centreline, the results obtained with this model come closer to the measured data than any other.

Utilization of Hydrodynamic Model B (test case 9) instead of Model A (test case 4) is not only a numerical, but also a physical modification. Looking at the momentum balances (see [2], [3] and [6], [7] in section 2.1), one can see that Model A and B would be identical if

$$-\nabla p = \frac{\beta}{\epsilon_G}(\mathbf{v}_G - \mathbf{v}_S). \qquad [42]$$

However, this is not true in this case. Especially in the fountain region, the pressure term in the vertical formulation of [42] is significantly higher than the corresponding drag term. Hence, if one takes the hydrostatic pressure gradient out of the solid phase momentum balance and instead increases the drag term, as done in Model B, the forces carrying particles into the freeboard are artificially decreased. Although theoretically the hydrostatic pressure is identical in both phases and hence Model A is physically more correct than Model B, the latter is able to predict results closer to the experiments for the present situation. A modification of the drag function β to account for non-homogeneous distribution of particles in a computational cell might overcome this problem.

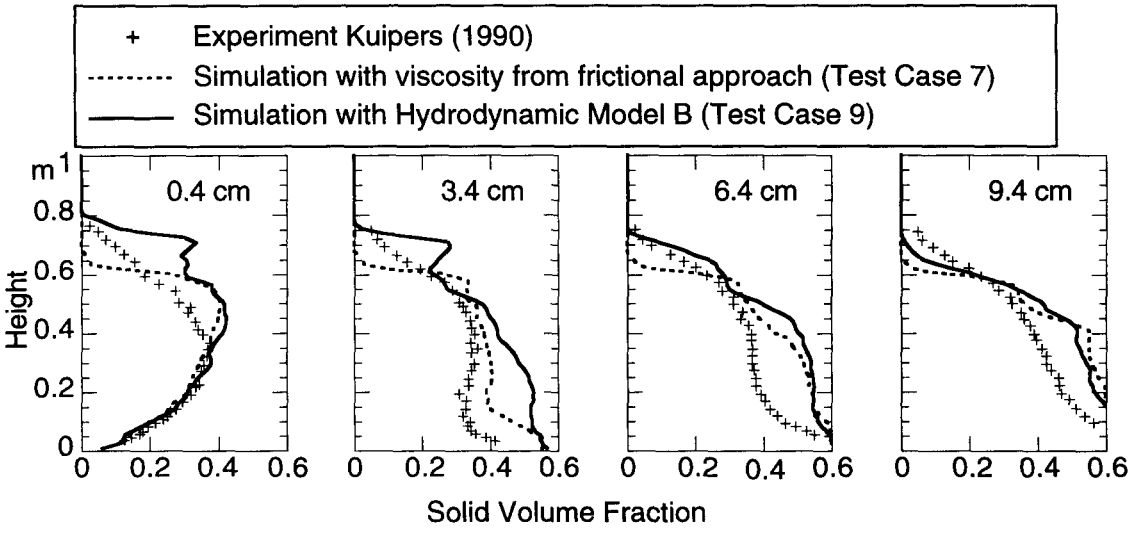

Figure 7. Time-averaged solid volume fractions at different distances from the centerline, proposals to overcome the fountain problem.

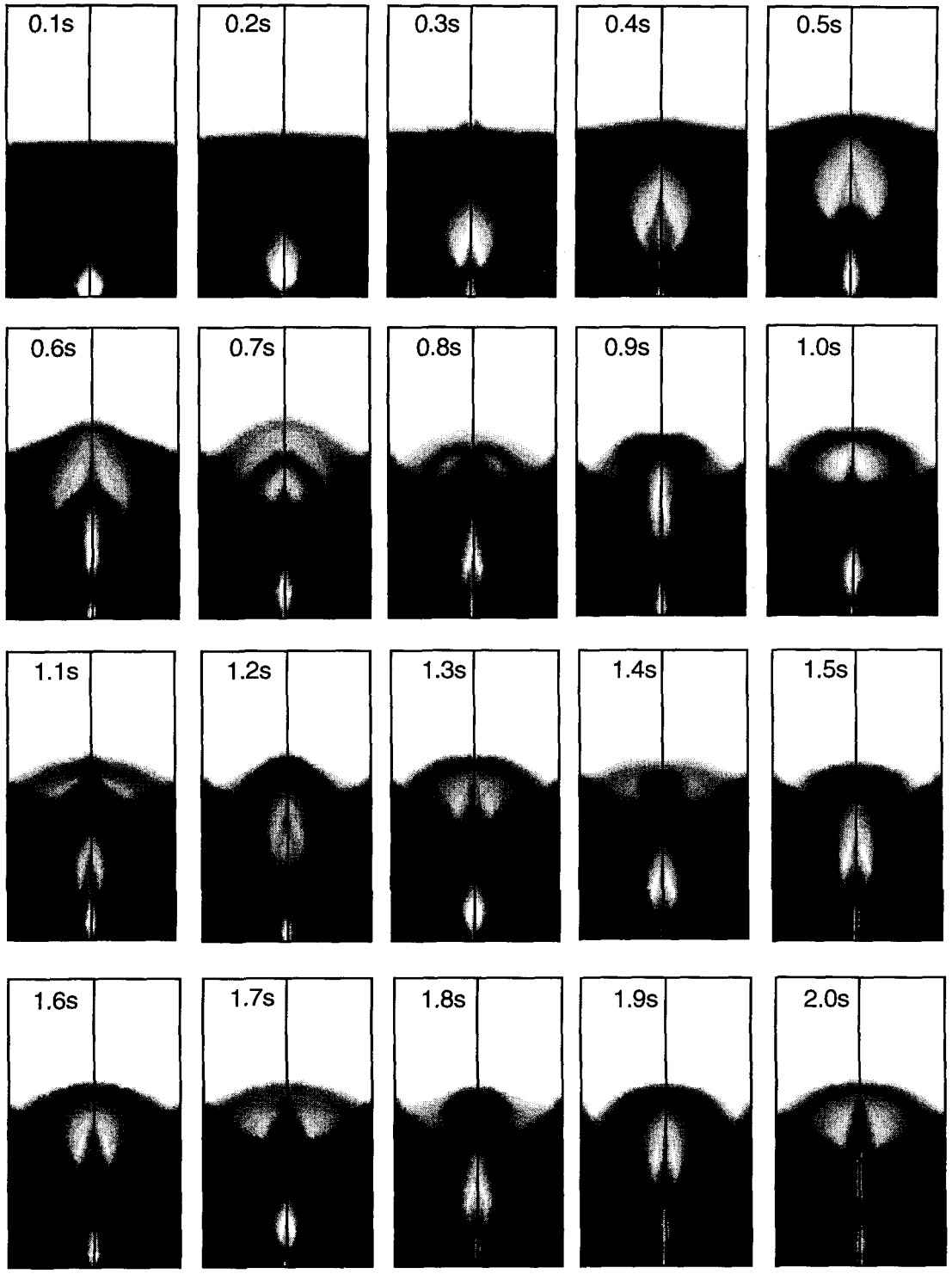

Figure 8. Process of bubble eruption, test case 7.

Kuipers (1990) successfully simulated the same test case with Model A, constant viscosities, and an empirically derived elastic modulus instead of solid pressure. Such a model is similar to the procedure described above with a constant granular temperature (test cases 1 and 2, see table 1). Since it turned out that a good guess of that granular temperature value is crucial for the results,

it can be assumed that the choice of the empirical formula for the elastic modulus and that of the value of solids shear and bulk viscosity have a strong influence on the results.

As an example, the complete process of bubble eruption is shown in figures 8 for test case 7. After the ascend of the first big bubble shown also in figure 5, the downflowing particles near the walls impede the growth of the following bubbles. Hence, the second and all following bubbles are leaner and faster that the first one. This was observed both in the simulations and the experiment.

4. CONCLUSIONS

In the frame of the Eulerian approach, physical models derived from the kinetic theory of granular flows are able to describe the bubble formation process in fluidized beds. Comparisons with measurements show good agreement.

The description of the fluctuating energy in terms of the granular temperature is the basis of the solid phase models. Although a good guess of a constant granular temperature may lead to acceptable results, the algebraic formula [36] should be preferred. Theoretically, solution of the complete partial differential equation [25] gives the most accurate results, but in case of dense beds the resulting flow patterns are similar to those calculated with the algebraic equation.

Concerning the values needed to limit the granular temperature, a range of $10^{-5} < \Theta_S < 0.1$ m^2/s^2 was found for bubbling fluidized beds.

An approach derived from solid mechanics to account for interparticle friction, [20], is favourable in the very dense regime. It can keep particles from splashing too high into the freeboard. The maximum limit of [20] was found to have no significant influence on the overall results.

Acknowledgements—This work was supported by the European Commission JOULE II under contract JOU2-CT94-0452.

REFERENCES

Albråten, P. (1982) The dynamics of two phase flow. Ph.D. thesis, Department of Energy Conversion, Chalmers University of Technology, Sweden.

Alder, B. J. and Wainwright, T. E. (1960) Studies in molecular dynamics. II: Behaviour of a small number of elastic spheres. *J. Chem. Phys.* **33,** 1439–1451.

Andersson, S. (1991) Dimensionless groups in the momentum equation of a bubbling fluidized bed. Chalmers University of Technology, Sweden, Report A 91–188.

Balzer, G. and Simonin, O. (1993) Extension of Eulerian gas–solid flow modelling to dense fluidized bed. *Proc. 5th Int. Symp. on Refined Flow Modelling and Turbulence Measurements*, ed. P. L. Viollet, pp. 417–424.

Boemer, A., Qi, H., Renz, U., Vasquez, S. and Boysan, F. (1995) Eulerian computation of fluidized bed hydrodynamics—a comparison of physical models. *Proceedings of the 13th Int. Conf. on FBC*, Orlando, pp. 775–786.

Bouillard, J. X., Lyczkowski, R. W. Gidaspow, D. (1989) Porosity distributions in a fluidized bed with an immersed obstacle. *AIChE Journal* **35,** 908–922.

Campbell, S. C. and Wang, D. G. (1991) Particle pressure in gas-fluidized beds. *J. Fluid Mech.* **227,** 495–508.

Carnahan, N. F. and Starling, K. E. (1969) Equations of state for non-attracting rigid spheres. *J. Chem. Phys.* **51,** 635–636.

Chapman, S. and Cowling, T. G. (1970) *The Mathematical Theory of Non-uniform Gases*, 3rd edn. Cambridge University Press, Cambridge.

Dalla Valle, J. M. (1948) *Micromeritics*. Pitman, London.

Dasgupta, S., Jackson, R. and Sundaresan, S. (1993) Turbulent gas-particle flow in CFB risers. *Proceedings of the 4th Int. Conf. on CFB*, Somerset, USA, Preprint Volume, pp. 448–453.

Di Felice, R. (1994) The voidage function for fluid-particle interaction systems. *Int. J. Multiphase Flow* **20,** 153–159.

Ding, J. and Gidaspow, D. (1990) A bubbling fluidization model using kinetic theory of granular flow. *AIChE Journal* **36,** 523–538.

Gamwo, I. K., Gidaspow, D., Lyczkowski, R. W. and Soong, Y. (1995) Three-dimensional hydrodynamic modeling of a bubbling fluidized bed. *Proceedings of the 13th Int. Conf. on FBC*, Orlando, pp. 297–303.

Garside, J. and Al-Dibouni, M. R. (1977) Velocity–voidage relationship for fluidization and sedimentation. *I&EC Proc. Des. Dev.*, **16,** 206–214.

Geldart, D. (1973) Types of gas fluidization. *Powder Technology* **7,** 285–292.

Gidaspow, D., Bezburuah, R. and Ding, J. (1992) Hydrodynamics of circulating fluidized beds; kinetic theory approach. *Fluidization VII, Proceedings of the 7th Engineering Foundation Conference on Fluidization*, pp. 75–82.

Gidaspow, D., Tsuo, Y. P. and Luo, K. M. (1989) Computed and experimental cluster formation and velocity profiles in circulating fluidized beds. *Fluidization VI, Proceedings of the 6th Engineering Foundation Conference on Fluidization.*

Gidaspow, D. (1994) *Multiphase Flow and Fluidization—Continuum and Kinetic Theory Descriptions* Academic Press, San Diego.

Grace, J. R. and Lim, C. J. (1987) Permanent jet formation in beds of particulated solids. *Can. J. Chem. Eng.* **65,** 160–162.

Jackson, R. (1983) Some mathematical and physical aspects of continuum models for the motion of granular materials. In *Theory of Dispersed Multiphase Flow*, ed. R. E. Meyer. Academic Press, New York.

Jenkins, J. T. and Savage, S. B. (1983) A theory for the rapid flow of identical, smooth, nearly elastic spherical particles. *J. Fluid Mech.* **130,** 187–202.

Johnson, P. C. and Jackson, R. (1987) Frictional–collisional constitutive relations for granular materials, with application to plane shearing. *J. Fluid Mech.* **176,** 67–93.

Kuipers, J. A. M. (1990) A two-fluid micro balance model for fluidized beds. Dissertation at the University of Twente, The Netherlands.

Löfstrand, H., Peirano, E. and Almstedt, A. E. (1995) Three-dimensional two-phase flow theory applied to fluidization, Publication Nr 95/2 at the Department of Thermo- and Fluid Dynamics, Chalmers University of Technology, Göteborg, Sweden.

Lun, C. K. K. and Savage, F. B. (1986) The effects of impact velocity dependant coefficient of restitution on stress developed by sheared granular materials. *Acta Mechanica* **63,** 15–44.

Lun, C. K. K., Savage, F. B., Jeffrey, D. J. and Chepurniy, N. (1984) Kinetic theories for granular flow: inelastic particles in couette flow and slightly inelastic particles in a general flowfield. *J. Fluid Mech.* **140,** 223–256.

Ma, D. and Ahmadi, G. (1990) A thermodynamical formulation for dispersed multiphase turbulent flows. *Int. J. Multiphase Flow* **16,** 323–351.

Massoudi, M., Rajagopal, K. R., Ekmann, J. M. and Mathur, M. P. (1992) Remarks on the modelling of fluidized systems. *AIChE Journal* **38,** 471–472.

Mih. W. C. (1993) An empirical shear stress equation for general solid–fluid mixture flows. *Int. J. Multiphase Flow* **19,** 683–690.

Moseley, J. L. and O'Brien, T. J. (1993) A model for agglomeration in a fluidized bed. *Chem. Engng Sci.* **48,** 3043–3050.

O'Brien, T. J. and Syamlal, M. (1993) Particle cluster effects in the numerical simulation of a circulating fluidized bed. Preprint Volume of the 4th Int. Conf. on CFB, Somerset, USA, pp. 430–435.

Patankar, S. V. (1980) *Numerical Heat Transfer and Fluid Flow*. Hemisphere, New York.

Pita, J. A. and Sundaresan, S. (1991) Gas–solid flow in vertical tubes. *AIChE Journal* **37,** 1009–1018.

Richarson, J. F. and Zaki, W. N. (1954) Sedimentation and fluidisation: Part I. *Trans. Instn Chem. Engrs* **32,** 35–52.

Savage, S. B. and Jeffrey, D. J. (1981) The stress tensor in granular flow at high shear rates. *J. Fluid Mech.* **110,** 255–272.

Sokolovski, V. V. (1965) *Statics of Granular Media*. Pergamon Press, Oxford.

Spalding, D. B. (1980) Numerical computation of multi-phase fluid flow and heat transfer. In *Recent Advances in Numerical Methods in Fluids*, ed. C. Taylor *et al.*, pp. 139–167. Pineridge Press.

Syamlal, M. and O'Brien, T. J. (1989) Computer simulation of bubbles in a fluidized bed. *AIChE Symp. Ser.* **85,** 22–31.

Syamlal, M., Rogers, W. and O'Brien, T. J. (1993) MFIX documentation, Theory Guide, Technical Note DOE/METC-94/1004.

Yang, Y.-L., Jin, Y., Yu, Z.-Q., Zhu, J.-X. and Bi, H.-T. (1993) Local slip behaviours in the circulating fluidized bed. *AIChE Symp. Series* **296,** 81–90.